# Carrier dynamics and saturation effect in (113)B InAs/InP quantum dot lasers

**K. Veselinov [1 *], F. Grillot[1], P. Miska [2 †], E. Homeyer [1], P. Caroff [1], C. Platz [1], J. Even [1], X. Marie [3], O. Dehaese [1], S. Loualiche [1] and A. Ramdane [4]**

(1) Laboratoire d'Etude des Nanostructures à Semiconducteurs, UMR CNRS 6082 Institut National des Sciences Appliquées, 20 avenue des buttes de Coesmes, 35043 Rennes Cedex, France

(2) Laboratoire de Physique des Matériaux,UMR CNRS Université Henri Poincaré Nancy I, Bvd des Aiguillettes, BP 239, F-54506 Vandoeuvre-lès-Nancy, France

(3) Laboratoire de Nanophysique, Magnétisme et Optoélectronique, INSA, 135 Avenue de Rangueil 31077 Toulouse, France

(4) Laboratoire de Photonique et Nanostructures, UPR CNRS 20, Route de Nozay, 91460 Marcoussis, France

( *author for correspondence: E-mail: kiril.veselinov@ens.insa-rennes.fr)



***Abstract***

Quantum dot (QD) lasers exhibit many interesting and useful properties such as low threshold current, temperature insensitivity or chirpless behavior. In order to reach the standards of long-haul optical transmissions, 1.55 µm InAs QD lasers on InP substrate have been developed. Based on time resolved photoluminescence (PL) measurements, carrier dynamics behavior is at first investigated. Electroluminescence (EL) results are then shown at room temperature exhibiting a laser emission centered at 1.61 µm associated to a threshold current density as low as 820 A/cm² for a six InAs QD stacked layers. Finally, a rate equation

† Previously at Laboratoire d'Etude des Nanostructures à Semiconducteurs

model based on the reservoir theory is used to model both time-resolved photoluminescence (TRPL) and electroluminescence results. It is shown that carrier dynamic calculations are in a good agreement with measurements since the saturation effect occurring at high injected power is clearly predicted.

***Key-words:*** semiconductor laser, quantum dots, carrier dynamics, rate equation

**Introduction**

While optics has proven to be the most practical response to the high traffic rate demand for long-haul transmission, its extension to the metropolitan networks down to the home remains an open challenge. The implementation of optics at transmission rate where other technical solutions exist requires cost reduction. As a consequence, semiconductor lasers based on low dimensional heterostructures such as quantum dots (QDs) laser are very promising. Indeed, QDs structures have attracted a lot of attention in the last decade since they exhibit many interesting and useful properties such as low threshold current, temperature insensitivity, chirpless behavior and optical feedback resistance. As a result, thanks to QDs lasers, several steps toward cost reduction can be reached such as: improving the laser resistance to temperature fluctuation in order to remove temperature control elements, or designing feedback resistant laser for isolator-free and optics-free module. Most investigations reported in the literature deal with In(Ga)As QDs grown on GaAs substrates (Tan et al. 2004, Mukai et al. 1999). It is however important to stress that In(Ga)As / GaAs QDs devices do not allow a laser emission above 1.35 µm which is detrimental for optical transmission. In order to reach the standards of long-haul optical transmissions, laser devices emitting at 1.55 µm are required. To fulfill this condition InAs QD lasers grown on InP substrate are used. For instance, 1.5 µm InAs QDs lasers grown on InAs(100) substrate have recently been reported

(Lelarge et al. 2005). They have demonstrated a modal gain as large as 64 $cm^{-1}$ in pulsed mode and a threshold current as low as 15 mA under continuous wave for buried ridge stripe laser.

In this paper, InAs QDs grown on InP(113B) substrate are investigated. It has been shown that growth on high index substrates such as (113)B, favors the achievement of a higher density of smaller QDs than on (100) InP substrates (Caroff et al. 2005). In order to optimize laser performances, the "double cap" (DC) growth method (Paranthoen et al. 2001) is used. Thanks to this method, a direct control of the QD height is obtained as well as the tuning of the device wavelength. Thus, based on laser structures containing such dots grown trough the DC procedure, a laser emission on the ground state (GS) has been first observed at room temperature under optical pumping (Paranthoen et al. 2002). In order to replace the InP first cap layer by GaInAsP quaternary alloy with gap emission wavelength of 1.18 µm a new DC QD growth procedure has been recently proposed (Caroff et al. 2005). As a result, QD laser structures also exhibit a laser emission but under electrical pumping (EP) at room temperature (Platz et al. 2005). The goal of this paper is devoted to present time-resolved photoluminescence (TRPL) and electroluminescence (EL) results recently obtained on InAs QDs structures grown on InP(113B). Experimental results are also compared to calculations derived from a numerical model. Let us note that a considerable work has already been devoted to model QD lasers based on InAs/GaAs system, consistent with TRPL (Bimberg et al. 1997) and EL measurements (Bhattacharyya et al. 1999, Sugawara et al. 2000).

The paper is organized as follows: in section 1, the two studied structures are described: a single QD layer sample and an edge emitting laser diode. In section 2, experimental results are presented and discussed. On one hand, TRPL optical characterizations are conducted using the single QD layer structure. Thus, investigating carrier dynamics, a saturation effect attributed to an efficient carriers relaxation to the QD-GS is demonstrated. On the other hand,

EL measurements are done at room temperature on the edge emitting laser, yielding an emission centered at 1.61µm. In section 3 numerical simulations based on a rate equation model (REM) are conducted. Self-consistent calculations in qualitative agreement with TRPL and EL measurements are presented. Our results and conclusions are summarized in the last section.

## 1. Description of the structures

### 1.1. Sample structure for optical characterization

An InAs QD layer is grown by gas-source molecular beam epitaxy on InP(113)B substrate at 480°C. In order to control the QDs maximum height, and to reduce their inhomogeneous size dispersion, the "double cap" growth method described in (Paranthoen et al. 2003) is applied by the deposition of a thin InP layer of about 2.5 nm. The dot lateral dimensions (average diameter 32 nm) are determined by atomic force microscopy (AFM) measurements before the capping procedure and remain unchanged after it (Miska et al. 2002). The QD density is 5 x $10^{10}$ $cm^{-2}$. The sample is finally covered by a second InP cap layer for optical characterizations. Fig. 1 shows a schematic drawing of this sample.

### 1.2. Electrically pumped laser structure

The laser structure was obtained using a refined DC QD growth procedure in which the InP first cap layer has been replaced by a GaInAsP quaternary material (Q1.18). The optimization of this refined method has already been reported elsewhere (Caroff et al. 2005, p. 358) . The active region is made of six layers of InAs DC QDs, which are covered by a 2 nm Q1.18 first cap and separated from each other by a 20 nm Q1.18 spacer. The same material is used to stake out the waveguide region by two 130 nm layers. Then, the laser cavity is clad by 0.5 µm of InP, which is n-doped on the substrate side and p-doped on the top side. Broad area lasers

with 30 µm, 50 µm and 100 µm stripe widths have been processed. The laser structure was cleaved into cavity lengths ranging from 0.45 mm to 2.15 mm whereas back and rear facets are uncoated. The laser structure is depicted in fig. 2.

## 2. Experimental results

### 2.1. Time-resolved photoluminescence results

To investigate the time evolution of the radiative states populations kinetic photoluminescence measurements have been realized. The sample described in section 1.1 was characterized by TRPL at low temperatures using a 790 nm Ti-sapphire laser, producing 1.2 ps long light pulses with a repetition rate of 82 MHz (Miska et al. 2002). In fig. 3, PL intensity related to the GS is plotted versus time at 10 K after pulsed excitation. Two different incident powers are investigated: 40W/cm² and 1200W/cm². It is important to stress that in both cases the GS population rise time is less than 100 ps, which is attributed to an efficient carrier relaxation into the QDs (Miska et al. 2003). Then a GS peak emission is detected for the low excitation power (white squares) showing a nearly exponential decay. In contrast for about 500 ps after excitation, a saturation effect occurs for the high injection rate curve (black squares) corresponding to the total filling of the available QD ground states. In that case, the decrease of the PL signal is not exponential. Thus, under high excitation density, QDs and WL electronic states are filled and their optical emission can be observed (Miska et al. 2003).

### 2.2. Electroluminescence results under pulsed excitation

EL measurements allow to study the optical power evolution of a semiconductor laser diode as a function of the electrical current density under pulsed electric excitation at room temperature. The laser structure has been presented in section 1.2. The electrical pulse width is 0.1 µs with a duty cycle of 0.1%. In fig. 4, EL spectra are shown for different values of

injection current density. Below threshold ((case a) 790 A/cm$^2$) spontaneous emission from InAs QDs gives rise to a wide spectrum. At threshold ((case b) 820 A/cm$^2$), a laser emission occurs on the GS transition centered at 0.77 eV (1.61 µm). Above threshold, and when increasing the injection current densities ((case c) 833 A/cm$^2$) the stimulated emission spectrum narrows. It is important to stress that no blue shift is observed in fig. 4 for the laser peak (dashed line). However, as the emission wavelength is equal to 1.61 µm the growth of QD stacked layers should be further optimized to reach a laser emission closed to 1.55 µm (Platz et al. 2005). In fig .4, the measured output light power is depicted in inset as a function of the current density. The threshold current density of the optimized QD laser structure is estimated to 820 A/cm$^2$ for a FP cavity length of 1.44 mm. This value corresponds to a threshold current density per QD layer of 137 A/cm$^2$ which is close to the best results ever reported for InAs/GaAlInAs QD lasers on InP(113)B substrate (Saito et al. 2001).

### 3. Numerical modeling

In the following, a numerical model is used to study carrier dynamics in a QD laser. Its active region consists of a QD ensemble, where different dots are interconnected by a wetting layer (WL). In this ensemble, two energy levels are assumed: a two-fold degenerate GS and a four-fold degenerate excited state (ES) (Miska et al. 2002). It is also assumed that there is only one QD ensemble, i.e., all dots have the same size (the inhomogeneous broadening is neglected). Electrons and holes are considered to be captured and emitted in pairs. Carriers are supposed to be injected directly from the contacts into the WL levels, so the barrier dynamics are not taken into account in the model. Based on the reservoir theory used for bulk, quantum well (Coldren et al. 1995) and for InAs/GaAs QDs (Berg et al. 2001) devices, a carrier reservoir having an appropriate volume has been here associated to each energy state (fig. 5). The volume of the photon reservoir $V_p$ is related to the optical confinement factor: $\Gamma = V_a / V_p$ ,

with $V_a$ being the active region volume. Following the sketch in fig. 5 a rate equations system, normalized to the respective reservoir volume and describing the change in carrier densities of the three electronic energy levels, can be written as:

$$\frac{dN_W}{dt} = \frac{G}{V_W} + \frac{N_E}{\tau_W^E}\frac{V_D}{V_W} - \frac{N_W}{\tau_E^W} f_E - \frac{N_W}{\tau_G^W} f_G - \frac{N_W}{\tau_W^{sp}} \tag{1}$$

$$\frac{dN_E}{dt} = \frac{N_W}{\tau_E^W}\frac{V_W}{V_D} f_E + \frac{N_G}{\tau_E^G} f_E - \frac{N_E}{\tau_W^E} - \frac{N_E}{\tau_G^E} f_G - \frac{N_E}{\tau_E^{sp}} \tag{2}$$

$$\frac{dN_G}{dt} = \frac{N_W}{\tau_G^W}\frac{V_W}{V_D} f_G + \frac{N_E}{\tau_G^E} f_G - \frac{N_G}{\tau_E^G} f_E - \frac{N_G}{\tau_G^{sp}} - \Gamma v_g Sa\left(N_G - 2N_D\right) \tag{3}$$

The evolution of the photon density population S is described as follows:

$$\frac{dS}{dt} = \Gamma v_g Sa\left(N_G - 2N_D\right) - \frac{S}{\tau_p} + \beta_{sp}\Gamma\frac{N_G}{\tau_G^{sp}} \tag{4}$$

where $v_g$ is the group velocity, *a* the GS linear gain coefficient and $N_D$ is the total number of dots. The contribution of the GS spontaneous emission into the lasing mode is denoted by the coefficient $\beta_{sp}$ and $\tau_p = \frac{1}{v_g(\alpha_i + \alpha_m)}$ is the photon lifetime with $\alpha_i$ and $\alpha_m$ being the internal and mirror losses respectively. The photon generation term in equation (4) is described by the difference between stimulated emission $R_S^G$ and absorption $R_G^S$ rates such as:

$$R_S^G - R_G^S = v_g Sa\left(N_G - 2N_D\right) \tag{5}$$

In equations (1) – (3) $f_E$ and $f_G$ are the probability to find carrier at ES and GS respectively (Berg et al. 2001). Carriers are injected into the WL at a rate G. They are captured into the ES within a capture time $\tau_E^W$ or directly into the GS within the same time ( $\tau_G^W = \tau_E^W$ ). On the other hand carriers relax from the ES to the GS ( $\tau_G^E$ ). It is assumed that at low injection power, the

relaxation is phonon-assisted while the Auger effect dominates when the injection gets larger. Trough a phenomenological relation between these effects and carrier density in the WL, the corresponding times are given as (Berg et al. 2003):

$$\tau_G^W = \tau_E^W = \frac{1}{A_W + C_W N_W} \tag{6}$$

$$\tau_{\mathrm{G}}^{\mathrm{E}} = \frac{1}{\mathrm{A_E} + \mathrm{C_E N_W}} \tag{7}$$

where $A_W$ ($A_E$), $C_W$ ($C_E$) are the coefficients for phonon and Auger-assisted relaxation respectively, related to the WL and the ES. The spontaneous recombination times are set to be identical for carriers in the WL and the ES, but slower for the GS ($\tau_{\mathrm{W}}^{\mathrm{sp}} = \tau_{\mathrm{E}}^{\mathrm{sp}} < \tau_{\mathrm{G}}^{\mathrm{sp}}$) . Finally, carriers can thermally escape in a time $\tau_E^G$ from the GS to the ES and in a time $\tau_W^E$ from the ES to the WL. In what follows, the REM is applied to simulate TRPL and EL results.

## 4. Numerical results

At first TRPL experiments under non-resonant excitation at 10 K for the 2 nm InAs/InP(113)B DC QD sample are simulated. In this case the incident optical pulse is represented as a time dependent Gaussian function. The optical generation rate is $G(t) = P\exp\left(-\frac{t^2}{2w^2}\right)$ with $w$ being the full-width at half-maximum set to 1.2 ps and P the incident probe power in Watts. Phonon and Auger coefficients have been used as fitting parameters. Their values are estimated as follows: $A_W$ = 1.35 x $10^{10}$ $s^{-1}$, $C_W$ = 5 x $10^{-15}$ $m^3.s^{-1}$, $A_E$ = 1.5 x $10^{10}$ $s^{-1}$, $C_E$ = 9 x $10^{-14}$ $m^3.s^{-1}$. In fig. 6 the simulated curves (solid line) related to the PL intensity of the GS are plotted over the experimental data (open squares) for three values of incident power densities at 10 K. As it is clearly shown, those numerical results are in good agreement with measurements since the saturation effect occurring in the GS at high power densities is clearly predicted. The inset reports the simulated rise time of the PL curves

as a function of the pump power. It varies in the limits from nearly 80 ps for low values of the pump power to less than 10 ps at higher excitations illustrating the switching from phonon to Auger-assisted relaxation.

In order to investigate the properties of the InAs/InP(113)B QD device under electrical pumping, steady-state solutions of the REM model have been determined. Simulation of the lasing performance is shown in fig. 7 where the photon density *S* is reported as function of the injection current density *J*. The steady-state generation rate is $G = I/q$, with *I* being the injected current and q the electron charge  The other parameters are similar to those taken from our previous simulation. A single longitudinal mode emission is assumed. Also gain nonlinearities as well as dynamics and losses in the barrier are not taken into account. A classical evolution is predicted when stimulated emission is predominant above threshold. In fig. 7, threshold current density does not exceed 220 A/cm² for 820 A/cm$^2$ measured. Such a difference can be attributed to a lack of accuracy of the numerical model. Indeed, temperature dependence, gain nonlinearities as well the QDs size dispersion responsible for the inhomogeneous broadening of the laser spectra have not been taken into account yet.

**Conclusions**

In this paper, two InAs/InP(113)B QD structures have been made according to different "double cap" growth procedures. At first, optical characterizations conducted on the one QD layer structure have led to show a saturation effect occurring at high injected power which has been attributed after analysis to an efficient carriers relaxation into the dot's GS. Then, electroluminescence measurements conducted on QD broad area laser have shown an emission at room temperature at 1.61 µm with a threshold current density of 820 A/cm$^2$ for a Fabry-Perot cavity length of 1.44 mm. This value corresponds to a threshold current density per QD layer as low as 137 A/cm$^2$ which is close to the best results ever reported for

InAs/GaAlInAs QD lasers on InP(113)B substrate. Finally, a rate equation model based on the reservoir theory has been presented. On one hand, it has been shown that numerical results describing carrier dynamic behavior and the saturation effect are in a good agreement with TRPL measurements. On the other hand a threshold current density equal to 220 A/cm$^2$ has been predicted. This last value appears a little bit underestimated by comparison with electroluminescence measurements. As a conclusion, the next step to be done is to improve the numerical model so as to calculate more accurately the threshold current as well as to investigate the laser dynamic behavior under modulation.

**Acknowledgments**

This work was supported by SANDiE network of excellence (Self-Assembled semiconductor Nanostructures for new Devices in photonics and Electronics) and CREFID (Centre Régional Francophone d'Ingénierie pour le Développement) .

**References**

Berg T. and J. Mork, Applied Physics Letters, 82 3083, 2003.

Berg, T., S. Bischoff, I. Magnusdottir and J. Mork, IEEE Photonics Technology Letters, 13 541, 2001.

Bhattacharyya, D., E. A. Avrutin, A. C. Bryce, J. H. Marsh, D. Bimberg, F. Heinrichsdorff, V. M. Ustinov, S. V. Zaitsev, N. N. Ledentsov, P. S. Kop'ev, ZH. I. Alferov, A. I. Onischenko, and E. P. O'Reilly, IEEEJ. of Selected Topics in Quantum Electron., 5 648, 1999.

Bimberg, D., N. Kirstaedter, N. N. Ledentsov, ZH. I. Alferov, P. S. Kop'ev and V. M. Ustinov, IEEEJ. of Selected Topics in Quantum Electron., 3 196, 1997.

Caroff, P., N. Bertru, C. Platz, O. Dehaese, A. Le Corre and S. Loualiche, J. Cryst. Growth, 273 357, 2005.

Coldren L. and S. Corzine, Diode Lasers and Photonic Integrated Circuits, John Wiley, New York, 28, 1995.

Lelarge, F., B. Rousseau, F. Pommereau and A. Accard, The 17th Indium Phosphide and Related Materials Conference, Glasgow, 8 – 12 May 2005, TP-34, 2005.

Miska, P., J Even, C. Paranthoen, O. Dehaese, H. Folliot, S. Loualiche and M. Senes and X. Marie, Physica E, 17 56, 2003.

Miska, P., C. Paranthoen, J Even, O. Dehaese, H. Folliot, N. Bertru, S. Loualiche, M. Senes and X. Marie, Semicond. Sci. Technol. 17 L63, 2002.

Mukai, K., Y. Nakata, K. Otsubo, M. Sugawara, N. Yokoyama and H. Ishikawa, IEEE Photonics Technology Letters, 11 1205, 1999.

Paranthoen, C., N. Bertru, O. Dehaese, A. Le Corre, S. Loualiche and B. Lambert, Appl. Phys. Lett. 78 1751, 2001.

Paranthoen, C., N. Bertru, B. Lambert, O. Dehaese, A. Le Corre, J Even, S. Loualiche, F. Lissillour, G. Moreau and J. C. Simon, Semicond. Sci. Technol. 17 L5, 2002.

Paranthoen, C., C. Platz, G. Moreau, N. Bertru, O. Dehaese, A. Le Corre, P. Miska, J Even, H. Folliot, C. Labbé, G. Patriarche, J. C. Simon and S. Loualiche, J. Cryst. Growth 251 230, 2003.

Platz, C., C. Paranthoen, P. Caroff, N. Bertru, C. Labbé, J Even, O. Dehaese, H. Folliot, A. Le Corre, S. Loualiche, G. Moreau, J. C. Simon and A. Ramdane, Semicond. Sci. Technol., 20 459, 2005.

Saito, H., K. Nishi, Akio Kamei and Shigeo Sugou, Applied Physics Letters, 78 267, 2001.

Sugawara, M., K. Mukai, Y. Nakata and H. Ishikawa, Physical Reviw B, 61 7595, 2000.

Tan, K. T., C. Marinelli, M. Thompson, A. Wonfor, M. Silver, R. Sellin, R. Penty, I. White, M. Lammlin, N. Ledentsov, D. Bimberg, A. Zhukov, V. Ustinov and A. Kovsh, IEEE Photonics Technology Letters, 16 1415, 2004.

**Figure Captions**

Figure 1. Sample structure with one layer of DC QDs for optical characterization

1x1µm² AFM picture of a QD plane.

Figure 2. Schematic drawing of InAs/InP QD laser structure. The active region is made of six stacked layers of InAs QDs with 20 nm Q1.18 barriers, sandwiched between two 130 nm Q1.18 wave guiding layers.

Figure 3. Temporal profile of the DC dot sample after optical excitation. Detection of the peak emission of the GS for two power densities.

Figure 4. Room temperature EL emission spectra of the optimized QD broad area laser with six QD stacked layers under pulsed electrical excitation for three different current densities: a) 790 A/cm$^2$, b) 820 A/cm$^2$, c) 833 A/cm$^2$**.** The laser stripe width and the cavity length are 100 µm and 1.44 mm respectively. The inset shows the measured output light power as a function of the injected current density.

Figure 5. Schematic representation of the reservoir model with the carrier and photon transitions (arrows). $V_W$ is the WL volume, $V_D$ the total volume of QDs and $V_P$ the volume of the photon reservoir.

Figure 6. Simulated (solid lines) and measured (squares) TRPL spectra of the GS emission for 40 W/cm$^2$ a), 650 W/cm$^2$ b) and 1200 W/cm$^2$ c) excitation power densities. The inset shows calculated PL rise time as a function of the pump power.

Figure 7. Simulated photon density as a function of the polarization current density**.**

**Figure 1**

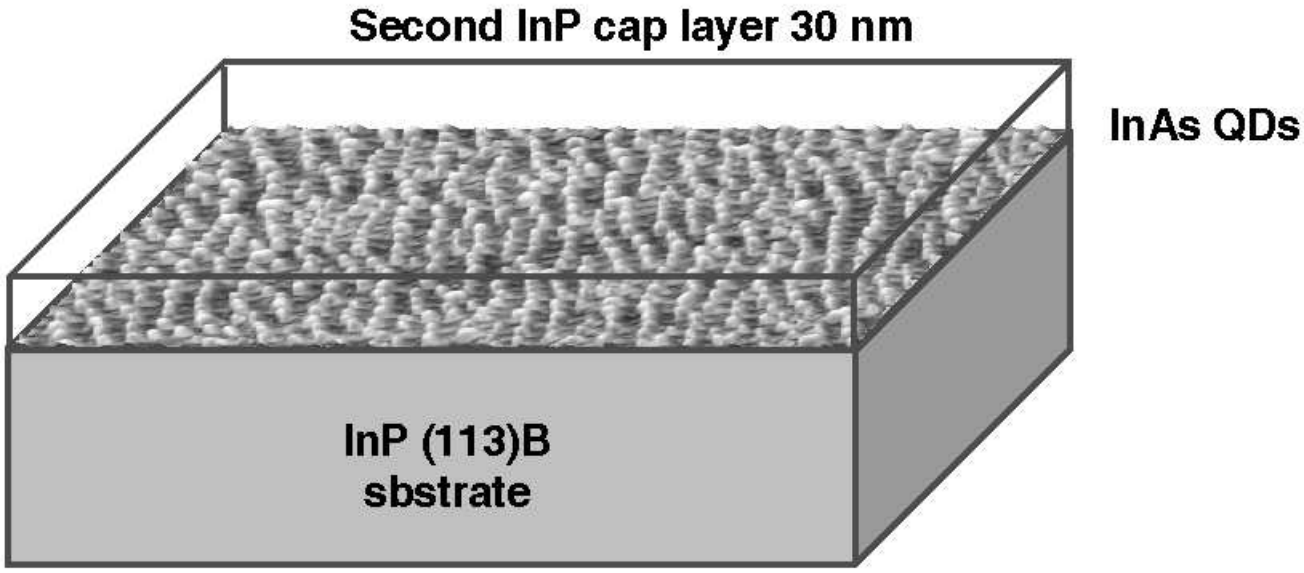

**Figure 2**

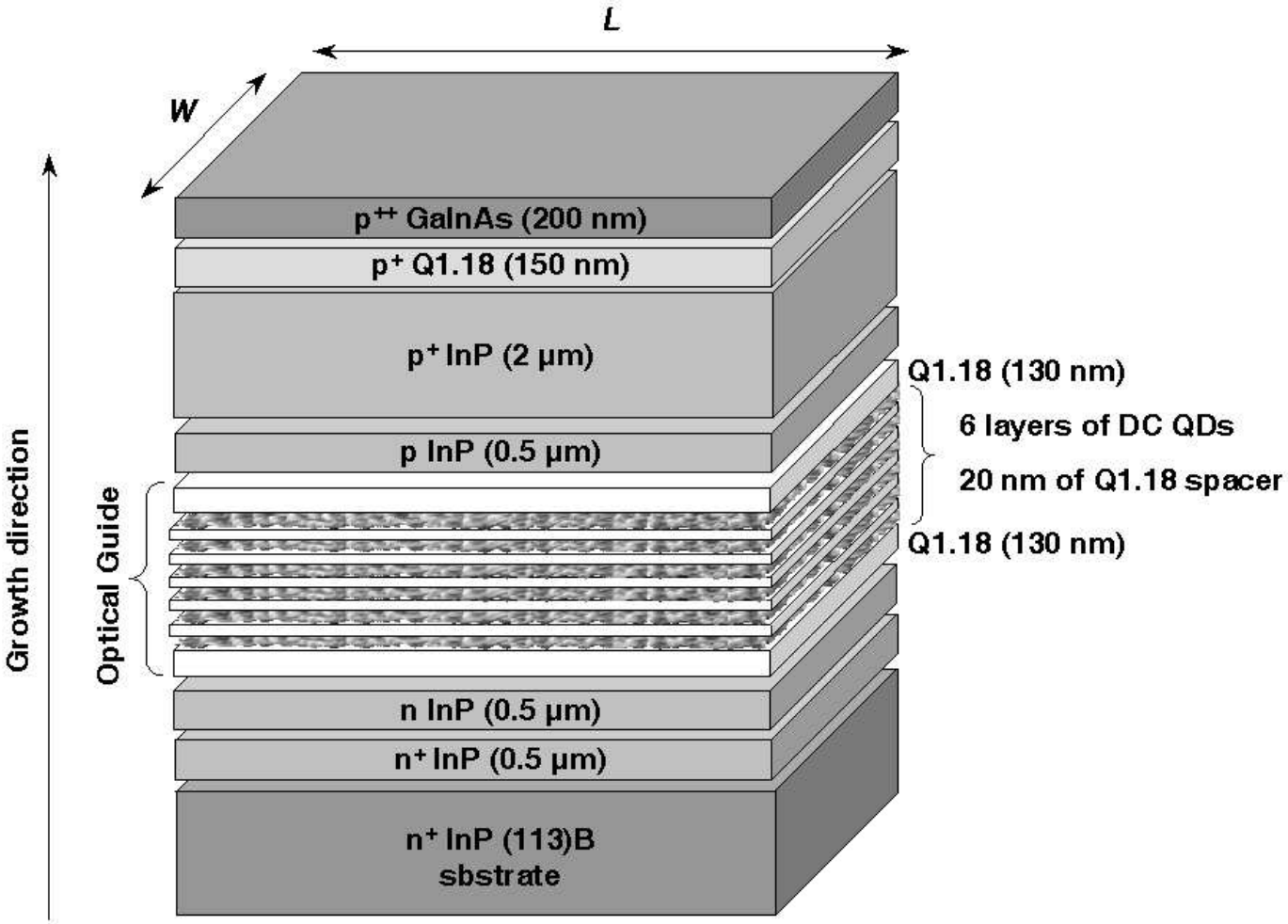

**Figure 3**

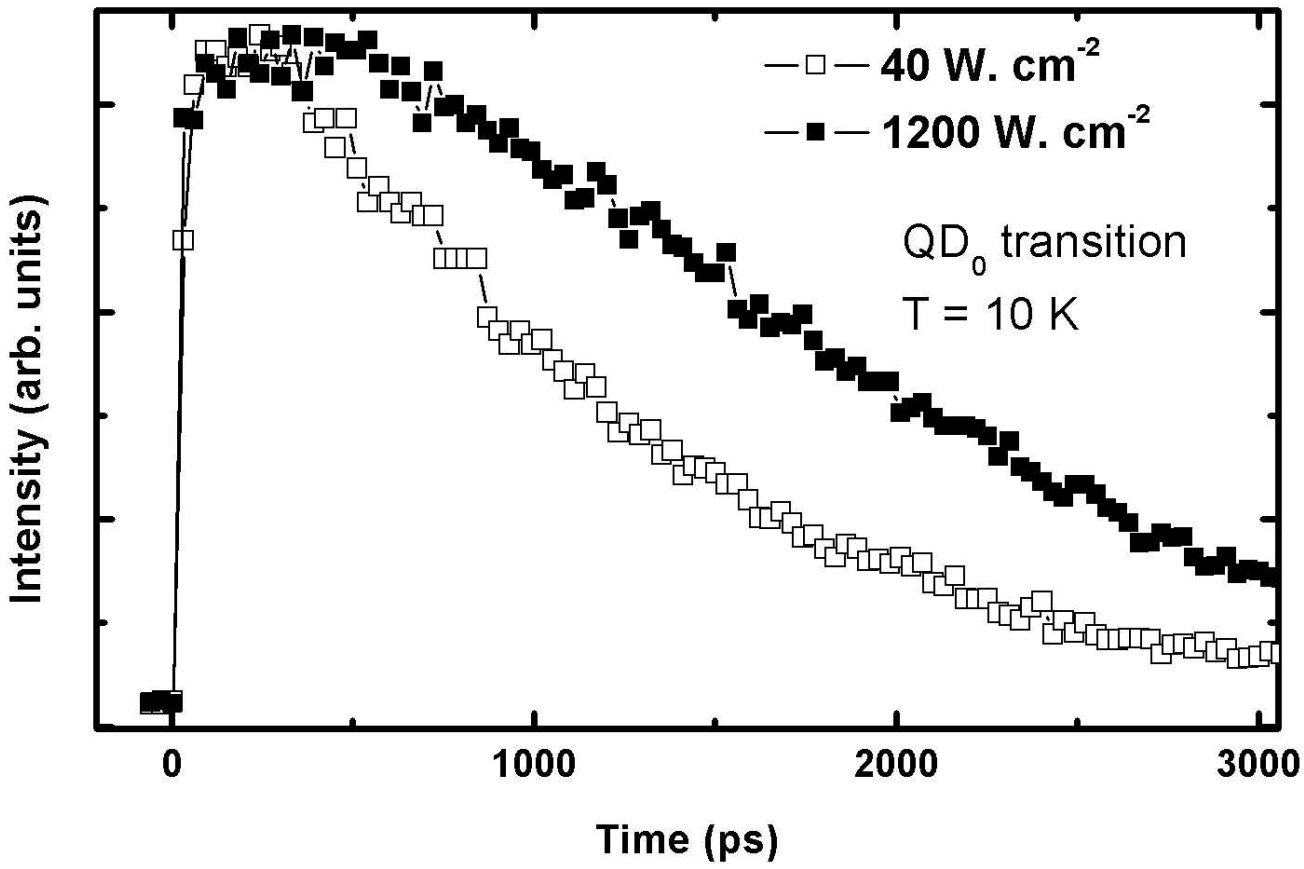

**Figure 4**

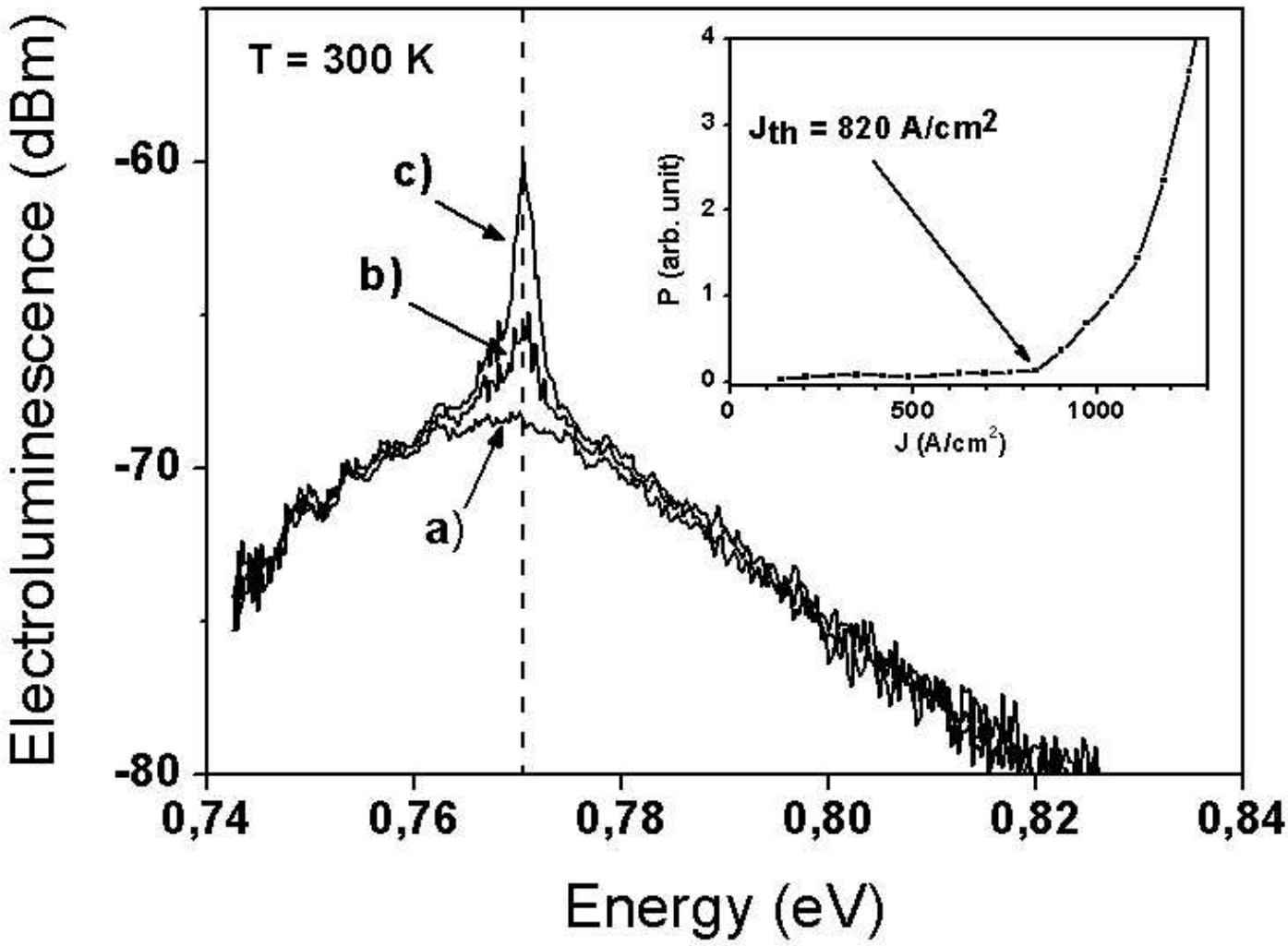

**Figure 5**

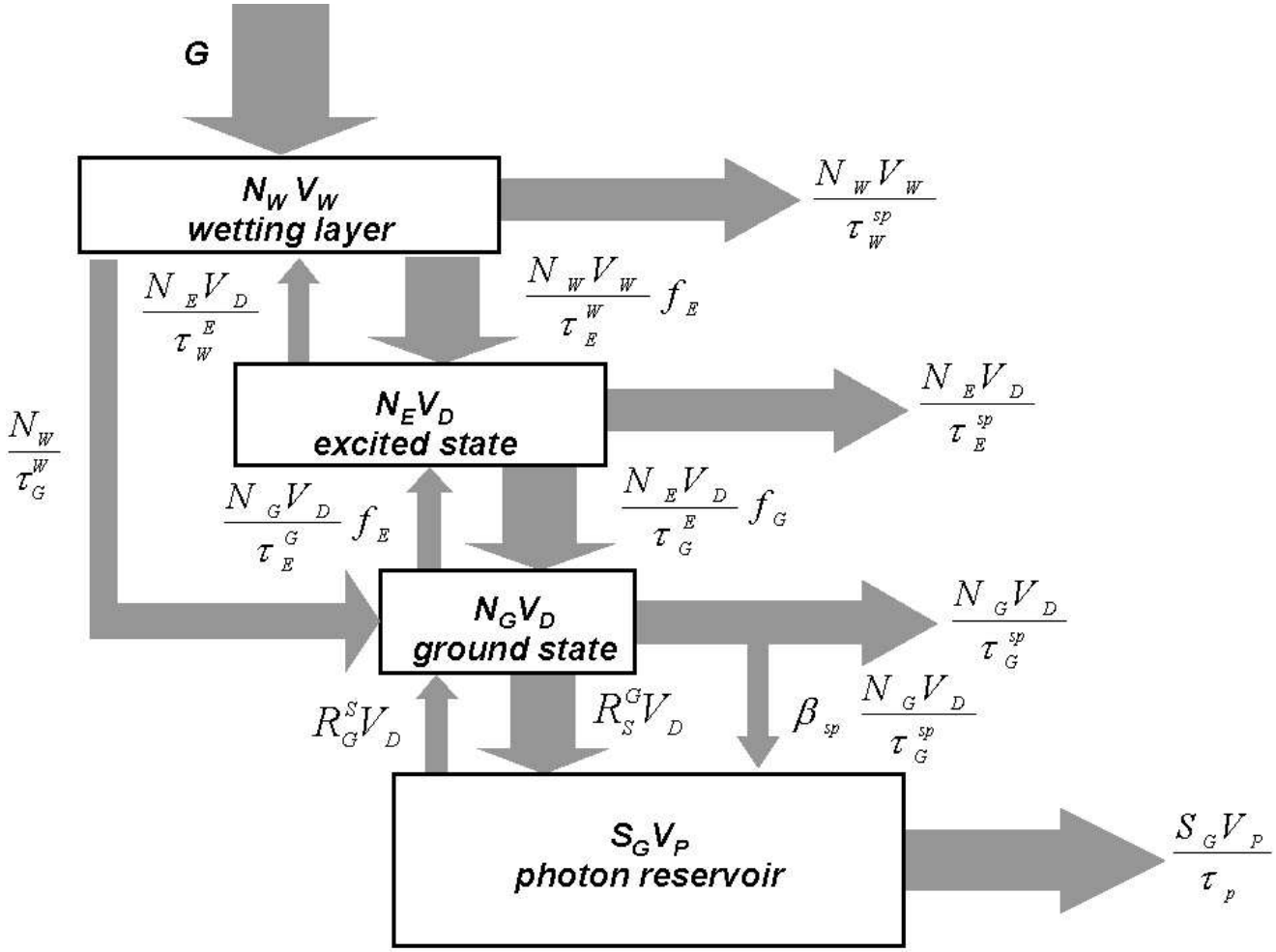

**Figure 6**

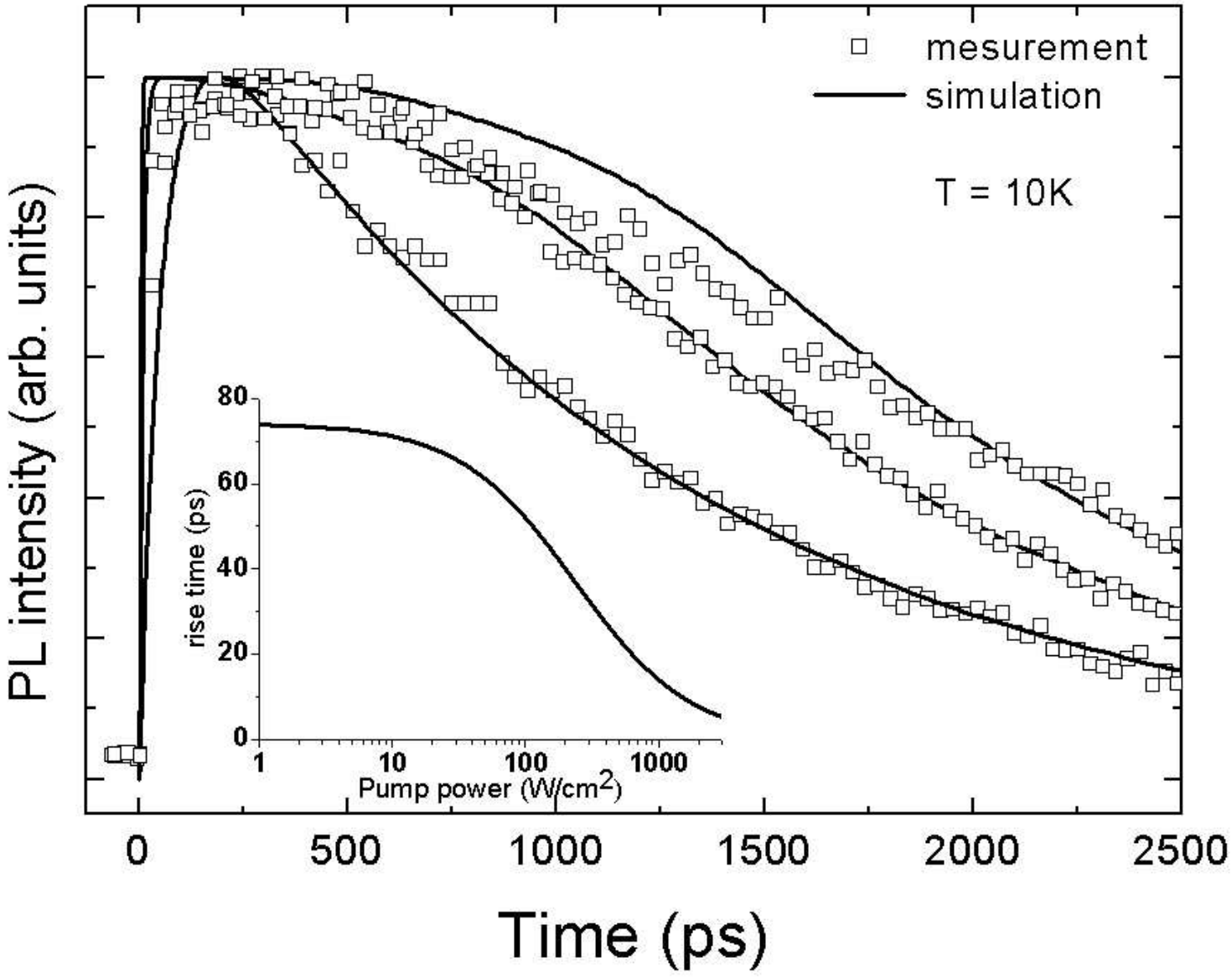

**Figure 7**